PROCEEDINGS OF THE ROYAL SOCIETY A MATHEMATICAL, PHYSICAL & ENGINEERING SCIENCES

A new phase-field model for strongly anisotropic systems

Solmaz Torabi, John Lowengrub, Axel Voigt and Steven Wise

Proc. R. Soc. A 2009 **465**, doi: 10.1098/rspa.2008.0385 first published online 13 January 2009

PROCEEDINGS OF THE ROYAL SOCIETY A

Proc. R. Soc. A (2009) **465**, 1337–1359
doi:10.1098/rspa.2008.0385
Published online 13 January 2009

A new phase-field model for strongly anisotropic systems

By Solmaz Torabi[1], John Lowengrub[1,2,*], Axel Voigt[3] and Steven Wise[4]

[1]*Department of Materials Science and Engineering, and* [2]*Department of Mathematics, University of California, Irvine, CA 92697-3875, USA*
[3]*Institut für Wissenschaftliches Rechnen, Technische Universität Dresden, 01062 Dresden, Germany*
[4]*Department of Mathematics, University of Tennessee, Knoxville, TN 37996-1300, USA*

We present a new phase-field model for strongly anisotropic crystal and epitaxial growth using regularized, anisotropic Cahn–Hilliard-type equations. Such problems arise during the growth and coarsening of thin films. When the anisotropic surface energy is sufficiently strong, sharp corners form and unregularized anisotropic Cahn–Hilliard equations become ill-posed. Our models contain a high-order Willmore regularization, where the square of the mean curvature is added to the energy, to remove the ill-posedness. The regularized equations are sixth order in space. A key feature of our approach is the development of a new formulation in which the interface thickness is independent of crystallographic orientation. Using the method of matched asymptotic expansions, we show the convergence of our phase-field model to the general sharp-interface model. We present two- and three-dimensional numerical results using an adaptive, nonlinear multigrid finite-difference method. We find excellent agreement between the dynamics of the new phase-field model and the sharp-interface model. The computed equilibrium shapes using the new model also match a recently developed analytical sharp-interface theory that describes the rounding of the sharp corners by the Willmore regularization.

Keywords: thin film; quantum dots; interfacial anisotropy; phase field; Cahn–Hilliard equations; Willmore regularization

1. Introduction

The formation of faceted pyramids on nanoscale crystal surfaces is an important phenomenon that has been attracting wide attention owing to its role in the self-organization of quantum dots. In crystalline films, these structures arise through competition among surface and bulk forces that result in instability. Instability may originate from a lattice misfit between film and substrate, from

* Author and address for correspondence: Department of Mathematics, University of California, Irvine, CA 92697-3875, USA (lowengrb@math.uci.edu).

Electronic supplementary material is available at http://dx.doi.org/10.1098/rspa.2008.0385 or via http://journals.royalsociety.org.

Received 23 September 2008
Accepted 9 December 2008

strong surface anisotropies or from kinetic surface fluxes. Facets on crystalline thin films, however, arise for a thermodynamic reason. In particular, such facets arise because the surface free energy is non-convex with respect to the surface normal (Herring 1951). Quantitative modelling of self-organization processes thus requires a detailed description of surface energies and mass transport mechanisms along the crystal surface.

Thermal faceting (spinodal decomposition) of thermodynamically unstable crystal surfaces caused by strongly anisotropic (non-convex) surface free energy densities and driven by surface diffusion has been considered in Stewart & Goldenfeld (1992), Liu & Metiu (1993) and Savina *et al.* (2003). However, all of these theoretical and numerical treatments are restricted to long-wave approximations based on small variations in surface orientation. This introduces a clear limitation in their quantitative predictive power as many experimentally observed facet angles in thin crystalline films are not small.

Only recently have numerical methods been proposed to deal with the full geometric evolution. The evolution law follows from a non-dimensional surface free energy of the form (Gurtin & Jabbour 2002)

$$E[\Gamma] = \int_\Gamma \gamma(\boldsymbol{n}) + \frac{\beta}{2} H^2 \, \mathrm{d}\Gamma, \tag{1.1}$$

with $\gamma(\boldsymbol{n})$ the classical surface free energy density with $\boldsymbol{n}$ the surface normal, H the mean curvature and $\sqrt{\beta}$ a small scale over which corners are smeared out. The energy can be viewed as a geometric Ginzburg–Landau-type energy with a non-convex functional and a gradient term. This is most apparent in the one-dimensional setting, where the energy can be written as $E[\Gamma] = \int_\Gamma \gamma(\theta) + (\beta/2)\,|\,\partial_s \theta\,|^2 \,\mathrm{d}\Gamma$ with θ the tangent angle (angle between the tangent vector $\boldsymbol{s}$ and the x-axis) and s is the arc length (Herring 1951; DiCarlo *et al.* 1992). Thus, it is also possible to interpret the gradient (curvature) term in equation (1.1) as the next higher order term in a more general surface free energy density $\tilde{\gamma} = \tilde{\gamma}(\boldsymbol{n}, H, \ldots) = \gamma(\boldsymbol{n}) + (\beta/2)H^2 + \cdots$.

The model we investigate here is the $\mathcal{H}^{-1}$ gradient flow of the energy (1.1). This leads to the (non-dimensional) surface diffusion equation

$$V = \Delta_\Gamma \nu \left(H_\gamma + \beta \left(\Delta_\Gamma H + \frac{1}{2} H^3 - 2KH \right) \right), \tag{1.2}$$

where V is the surface normal velocity; Δ_Γ is the surface Laplacian; ν is the mobility; H_γ is the weighted mean curvature; and K is the Gaussian curvature. The weighted mean curvature is defined through $H_\Gamma = \nabla \cdot \boldsymbol{\xi}$, where $\boldsymbol{\xi} = D\gamma(\boldsymbol{n})$ is the Cahn–Hoffman (1974) vector. When the surface energy is sufficiently anisotropic, equation (1.2) is ill-posed for $\beta = 0$. When $\beta > 0$, Siegel *et al.* (2004) and Hausser & Voigt (2005*a*) solved this highly nonlinear sixth-order equation numerically. However, both approaches are restricted to curves as severe numerical problems occur for evolving parametric surface meshes. A level-set approach circumventing some of these difficulties is discussed in Burger *et al.* (2007). Here, we are interested in a phase-field approximation of the problem. The phase-field method is capable of describing the evolution of complex, topology-changing surfaces and also provides a general framework to add further physical effects such as elasticity or compositional differences. In the phase-field approach, sharp interfaces are given a finite thickness and the energy (1.1) is modified appropriately. As such, this is also known as a diffuse-interface method.

Attempts towards a phase-field approximation have been made in Eggleston & Voorhees (2002), Wise *et al.* (2005, 2007), Rätz *et al.* (2006) and Wheeler (2006). However, none of these models approximate the geometric evolution described above in equation (1.2) correctly as the diffuse-interface width tends to zero. In an alternative phase-field approach, Eggleston *et al.* (2001) and Eggleston & Voorhees (2002) dealt with the ill-posedness of the anisotropic problem by convexifying the energy. This method does not reproduce equation (1.2) in the sharp-interface limit, and it also modifies the physics by suppressing the nucleation of new facets if the film is started with an orientation within the non-convex region (see Gurtin & Jabbour 2002; Fried & Gurtin 2004). Wise *et al.* (2005, 2007) and Wheeler (2006) used a regularization of the ill-posed equation based on adding the square of the Laplacian of the phase-field variable to the energy (instead of the mean curvature squared as shown above). This leads to a rounding of corners and edges and allows for spinodal decomposition of unstable orientations into stable ones. However, the asymptotic limit of the associated phase-field/diffuse-interface system is not equation (1.2) and the dynamics and equilibrium shapes of the two models are different.

A correct phase-field approximation of equation (1.2) requires an approximation of the Willmore energy. Attempts to construct phase-field approximations for the Willmore energy date back to De Giorgi (1991), who conjectured an appropriate approximation, which has since been analysed and simplified using different methods by Loreti & March (2000), Du *et al.* (2004, 2005), Röger & Schätzle (2006) and Wang (2007). An alternative approach has been used by Biben & Misbah (2003), Biben *et al.* (2005) and Jamet & Misbah (2008). In Rätz *et al.* (2006), the De Giorgi approach to approximating for the Willmore energy, which we follow in this paper, is proposed as a regularization for the strong anisotropic surface energy in a phase-field model. Adaptive numerical simulations using this approach were performed by Wise *et al.* (2007). However, the specific forms of the Willmore term and the phase-field/diffuse-interface approximation of the anisotropic surface energy term used in these works were incompatible. Thus, this approach also does not give equation (1.2) as the asymptotic limit. The incompatibility arises because of an inappropriate combination of anisotropic and isotropic terms in the energy. In particular, the orientation-dependent interface thickness introduced by the surface energy anisotropy (Kobayashi 1993) is not compatible with the Willmore approximation that assumes a uniform interface thickness. This motivated us to develop a new way of approximating anisotropic free energies in phase-field models. A key feature of our approach is a diffuse-interface thickness that is independent of the orientation. This makes it straightforward to combine isotropic and anisotropic terms. The resulting system is highly nonlinear and is sixth order in space.

Using matched asymptotic expansions, it can be shown that our new model converges to the classical sharp-interface model in the limit of vanishing interface thickness (see the electronic supplementary material). We present simulations in two and three dimensions, which show excellent agreement between the dynamics and equilibrium shapes simulated by the sharp-interface model and by our new phase-field model. At equilibrium, the computed shapes also match the results of an analytical sharp-interface theory by Spencer (2004), which describes the rounding of sharp corners by the Willmore regularization.

The paper is organized as follows. In §2, we discuss equilibrium shapes of crystals with strong anisotropies. In §3, we derive the phase-field model for the Willmore regularization of strongly anisotropic surface diffusion. In §4, we briefly describe the numerical scheme used to solve the highly nonlinear sixth-order phase-field/diffuse-interface equations. In §5, we present simulations of the evolution of facetted curves and surfaces. We compare the equilibrium shapes with the asymptotic results in Spencer (2004). We also demonstrate mound formation and the coarsening of surface structures. Finally we draw conclusions in §6. The formal matched asymptotic expansion showing the convergence to the sharp-interface model is given in the electronic supplementary material.

2. Equilibrium shapes

The equilibrium (Wulff) shape of a crystal is defined as the shape that minimizes the surface free energy $E[\Gamma]$ under the constraint of fixed enclosed volume. Depending on the details of the free energy density γ, the equilibrium shape may contain corners and edges. In such cases, it is energetically favourable to exclude high-energy orientations and allow for missing orientations. In two dimensions, the surface energy $\gamma(\boldsymbol{n})$ can be written as $\gamma=\gamma(\theta)$, where θ is the tangent angle. Corners, edges and missing orientations occur if the stiffness becomes negative for some orientations. The stiffness is defined as $\tilde{\gamma}=\gamma+\gamma_{\theta\theta}$. In three dimensions, with $\gamma=\gamma(\theta,\phi)$ depending on two angles, no such analytical criterion is known. Instead, the polar plot of $1/\gamma$ has to be used and it has been shown in Sekerka (2005) that the onset of missing orientations occurs at a convex-to-concave transition in the $1/\gamma$ plot. Using the Cahn–Hoffman (1974) $\boldsymbol{\xi}$-vector, missing orientations occur when 'ears' and 'flaps' form in the $\boldsymbol{\xi}$-plot (Sekerka 2005). Consider the fourfold symmetric model-type anisotropy

$$\gamma(\boldsymbol{n})=\gamma(\theta)=1+\alpha\left(4\sum_{i=1}^{d}n_i^4-3\right), \tag{2.1}$$

where α is the anisotropy strength and $d=2$, 3 is the space dimension. In two dimensions, this is equivalent to

$$\gamma(\boldsymbol{n})=1+\alpha\cos 4\theta. \tag{2.2}$$

In this paper, we use these anisotropy functions exclusively although our approach of course works for any such function. The anisotropy function (2.1) is convex for values $\alpha<1/15$ and non-convex for $\alpha\geq 1/15$. In figure 1, the corresponding Wulff shapes that are plotted (in three dimensions the $\boldsymbol{\xi}$-plot is shown), which in three dimensions resemble a double-sided pyramid, are shown for convex ($\alpha=0.06$) and non-convex ($\alpha=0.2$ and 0.3) surface energy functions γ from equation (2.1). Note that the actual Wulff shapes do not contain the unphysical ears and flaps (that appear in the three-dimensional $\boldsymbol{\xi}$-plot) and instead contain corners and missing orientations (e.g. Sekerka 2005).

The $\mathcal{H}^{-1}$ gradient flow of the corresponding surface energy $E[\Gamma]=\int_\Gamma\gamma(\boldsymbol{n})\,\mathrm{d}\Gamma$ defines the following model for anisotropic surface diffusion:

$$V=\Delta_\Gamma\left(\nu\frac{\delta E}{\delta\Gamma}\right), \tag{2.3}$$

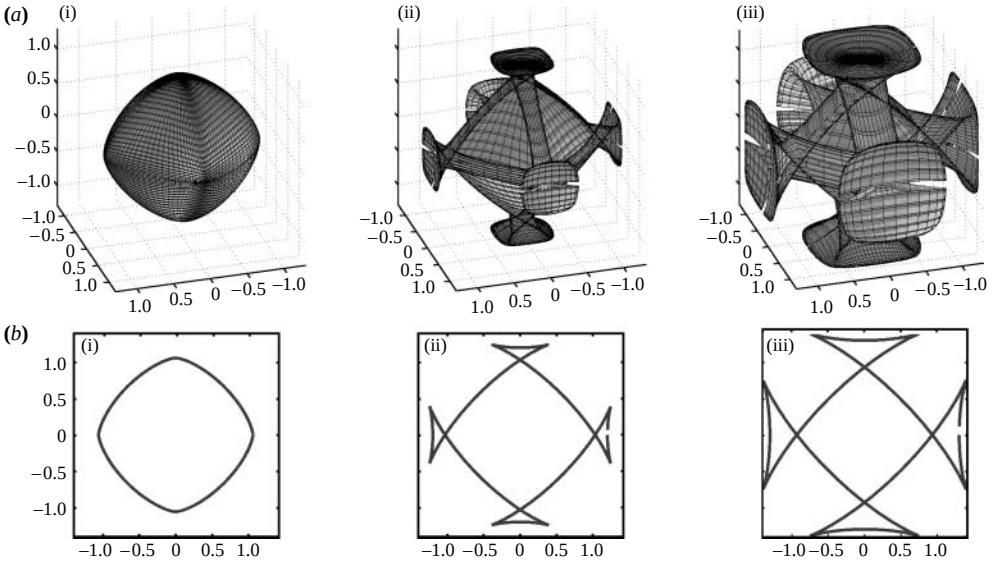

Figure 1. (*a*) Three- and (*b*) two-dimensional Wulff shapes with α as labelled. In three dimensions, the ξ-plot (Sekerka 2005) is shown. (i) $\alpha=0.06$, (ii) $\alpha=0.2$ and (iii) $\alpha=0.3$.

where Δ_Γ is the surface Laplacian (Laplace–Beltrami operator) and ν is the mobility. In two dimensions, $\Delta_\Gamma=\partial_{ss}$, where s is the arc length, and

$$\frac{\partial E}{\partial \Gamma}=(\gamma+\gamma'')H, \tag{2.4}$$

where $\gamma'=\mathrm{d}\gamma/\mathrm{d}\theta$. When the anisotropy is sufficiently strong such that there are missing orientations in the Wulff shape, the evolution by surface diffusion is inherently unstable. In fact, the evolution equations are actually ill-posed because the equations are backward parabolic for these orientations owing to the non-convexity of the anisotropic surface energy. One way to overcome this ill-posedness is to regularize the equation by adding a curvature-dependent term to the interface energy. This was already proposed on physical grounds in Herring (1951), and later mathematically introduced in DiCarlo *et al.* (1992) and Gurtin & Jabbour (2002). Such a curvature-dependent term introduces a new length scale on which sharp corners and edges are rounded. In Rätz & Voigt (2006), it is argued that even higher order terms in the energy are necessary to prevent a surface from forming corners and edges; however, here we will only consider energies as in equation (1.1). Minimizing the surface energy thus becomes a compromise between a large curvature at the corners and edges, which decreases orientations with large surface energy but increases the regularization term, and small curvature at the corner, which decreases the regularization term but increases orientations with large surface energy. The amount of corner rounding is therefore determined by these two competing energy terms. The plausibility of such a regularization is clear, but its effect on the equilibrium shape was only recently analysed for curves and is still open for surfaces. For curves, Spencer (2004) gave an asymptotic analysis that shows the convergence to the sharp-corner (Wulff) results as the regularization parameter $\beta\to 0$ and

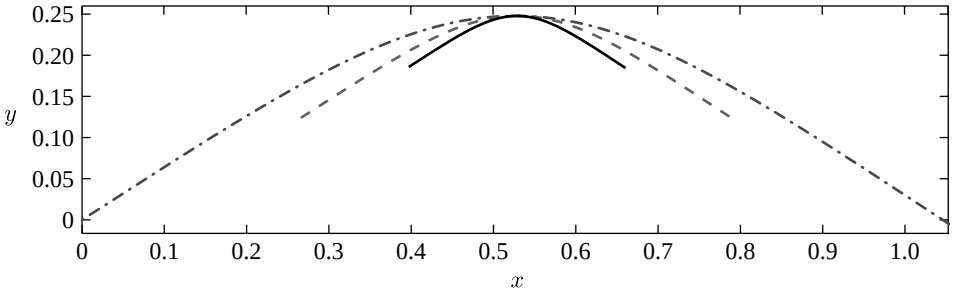

Figure 2. Close-up of a rounded corner with $\alpha=0.2$ and different Willmore regularization parameters; $\beta=0.04$ (dot-dashed curve), 0.01 (dashed curve) and 0.0025 (solid curve), following Spencer (2004).

provides an analytical formula for the equilibrium shape near a rounded corner for $\beta>0$ (figure 2). We will use this asymptotic solution, referred to as a regularized Wulff shape, later to compare with equilibrium corner profiles for the new phase-field/diffuse-interface model.

3. Phase-field/diffuse-interface approximation

In the phase-field/diffuse-interface approach, narrow transition layers replace sharp interfaces and an order parameter φ that denotes the phases in a multiphase system is introduced. The order parameter is constant (0 or 1) in each phase and the interface (transition layer) between phases corresponds to the region where φ varies from 0 to 1. The classical formulation of the phase-field/diffuse-interface equations for isotropic systems is based on the energy (Cahn & Hilliard 1958)

$$E[\varphi]=\int_{\Omega}\frac{1}{\epsilon}\left(f+\frac{\epsilon^2}{2}\,|\nabla\varphi\,|^{2}\right)\mathrm{d}\Omega, \tag{3.1}$$

where ϵ is a small parameter that is a measure of the interface transition layer thickness and $f=f(\varphi)$ is a double-well potential. A phase-field approximation for surface diffusion based on this energy was introduced by Cahn *et al.* (1996). The evolution law is

$$\frac{\partial\varphi}{\partial t}=\frac{1}{\epsilon}\,\nabla\cdot(M(\varphi)\nabla\mu), \tag{3.2}$$

$$\mu=\frac{1}{\epsilon}(f'(\varphi)-\epsilon^2\Delta\varphi), \tag{3.3}$$

where $M(\varphi)$ is the mobility which is localized near the interface, e.g. $M(\varphi)=4\varphi(1-\varphi)$. Equation (3.3) is a degenerate Cahn–Hilliard equation that converges as $\epsilon\to0$ to motion by surface diffusion $V=\Delta_{\Gamma}H$. An improved version has been given in Rätz *et al.* (2006), where μ is replaced by $G\mu$, with $G=G(\varphi)$ localized near the interface. A detailed asymptotic analysis for this and other approaches, not discussed here, is given in Gugenberger *et al.* (2008). In the isotropic case, numerical simulations indicate that using $G\mu$ rather than μ does not significantly

influence the evolution (A. Rätz & A. Voigt 2008, personal communication). Assuming that the double-well potential is $f(\varphi)=\varphi^2(1-\varphi)^2/4$, then in all cases the profile across the interfacial layer is

$$\varphi = \frac{1}{2}\left(1+\tanh\left(\frac{d}{2\sqrt{2}\epsilon}\right)\right), \tag{3.4}$$

where d denotes the signed distance to the centre of the interfacial layer. Following the classical approach to incorporate anisotropy (Kobayashi 1993), the anisotropic energy is

$$E[\varphi] = \int_\Omega \frac{1}{\epsilon}\left(f+\frac{\epsilon^2}{2}\,|\,\gamma(\boldsymbol{n})\nabla\varphi\,|^2\right)\mathrm{d}\Omega, \tag{3.5}$$

and the new evolution law for weak (convex) anisotropies reads

$$\frac{\partial\varphi}{\partial t} = \frac{1}{\epsilon}\,\nabla\cdot\left(\frac{1}{\gamma(\boldsymbol{n})}M(\varphi)\nabla\mu\right), \tag{3.6}$$

$$\mu = \frac{1}{\epsilon}(f'(\varphi)-\epsilon^2\nabla\cdot\boldsymbol{m}), \tag{3.7}$$

where the anisotropic gradient $\boldsymbol{m}$ is given by

$$\boldsymbol{m} = \gamma^2(\boldsymbol{n})\nabla\varphi + \gamma(\boldsymbol{n})\,|\nabla\varphi\,|\,\boldsymbol{P}\nabla_{\boldsymbol{n}}\gamma(\boldsymbol{n}), \tag{3.8}$$

and the unit normal $\boldsymbol{n}$ and the projection matrix $\boldsymbol{P}$ are given by

$$\boldsymbol{n} = \frac{\nabla\phi}{|\,\nabla\phi\,|},$$

and

$$\boldsymbol{P} = \boldsymbol{I}-\boldsymbol{n}\otimes\boldsymbol{n},$$

where $\boldsymbol{I}$ is the identity matrix. In equation (3.8), $\nabla_{\boldsymbol{n}}$ represents the gradient with respect to the components of the normal vector. In Rätz *et al.* (2006), the convergence of this model to motion by anisotropic surface diffusion $V=\Delta_\Gamma H_\gamma$ is shown by the method of matched asymptotic expansions as $\epsilon\to 0$. In this approach (see also Wheeler *et al.* 1996), the interface thickness is seen to be a function of orientation

$$\varphi = \frac{1}{2}\left(1+\tanh\left(\frac{d}{2\sqrt{2}\epsilon\gamma(\boldsymbol{n})}\right)\right). \tag{3.9}$$

Starting from these equations various attempts have been made to extend the approach outlined above to strongly anisotropic (non-convex) surface free energy densities γ. As in the sharp-interface case, equations (3.6)–(3.8) become ill-posed (e.g. Wise *et al.* 2007). Wise *et al.* (2005, 2007) and Wheeler (2006) used a regularization of the ill-posed equation based on the Laplacian of the phase-field variable, thus adding

$$\frac{\beta}{2}\int_\Omega \frac{1}{\epsilon^3}(\epsilon^2\Delta\varphi)^2\,\mathrm{d}\Omega \tag{3.10}$$

to the energy. In Rätz *et al.* (2006), an approach is proposed which uses instead a De Giorgi-type phase-field approximation of the Willmore energy as a regularization. In this case, the additional term in the energy is

$$\frac{\beta}{2}\int_{\Omega}\frac{1}{\epsilon^3}(f'(\varphi)-\epsilon^2\Delta\varphi)^2\,\mathrm{d}\Omega. \tag{3.11}$$

This was implemented and investigated in Wise *et al.* (2007). Such phase-field/diffuse-interface approximations of the Willmore energy have been shown to converge to the Willmore functional in the limit $\epsilon\to 0$ (see Loreti & March 2000; Du *et al.* 2004, 2005; Röger & Schätzle 2006; Wang 2007). However, it can be seen that the Willmore term leads to a constant interface thickness and is thus not compatible with the phase-field/diffuse-interface approximation of anisotropy as outlined above. In an alternative approach to approximating the Willmore energy, used in Biben & Misbah (2003), Biben *et al.* (2005) and Jamet & Misbah (2008), the curvature may be directly calculated by $H=\nabla\cdot\boldsymbol{n}$, with $\boldsymbol{n}$ given as above, and the integrand in equation (3.11) may be replaced with $H^2|\nabla\phi|$. While this approach is feasible to use here, it leads to additional nonlinearity compared with the De Giorgi approach.

We now reformulate the anisotropic energy (3.5) such that the interface thickness is independent of orientation. For this reason, we consider the anisotropic surface energy as

$$E[\phi]=\int_{\Omega}\frac{\gamma(\boldsymbol{n})}{\epsilon}\left(f+\frac{\epsilon^2}{2}\,|\nabla\varphi\,|^2\right)\mathrm{d}\Omega. \tag{3.12}$$

Note that this form of the energy differs from the form in equation (3.5) in that γ multiplies both the f and $|\nabla\varphi|^2$ terms. This is a natural formulation if we interpret the term $(1/\epsilon)(\,f(\varphi)+(\epsilon^2/2)\,|\nabla\varphi\,|^2)$ as approximating the surface delta function as in the original Cahn–Hilliard system. The corresponding evolution law becomes

$$\frac{\partial\varphi}{\partial t}=\frac{1}{\epsilon}\nabla\cdot(M(\varphi)\nabla\mu), \tag{3.13}$$

$$\mu=\frac{1}{\epsilon}(\gamma f'(\varphi)-\epsilon^2\nabla\cdot\boldsymbol{m}), \tag{3.14}$$

with

$$\boldsymbol{m}=\gamma(\boldsymbol{n})\nabla\varphi+\boldsymbol{P}\nabla_n\gamma(\boldsymbol{n})\left(\frac{f}{\epsilon^2\,|\,\nabla\varphi\,|}+\frac{1}{2}\,|\,\nabla\varphi\,|\right).$$

To further simplify, we may use the asymptotic result that near interfaces $f(\varphi)\sim(\epsilon^2/2)\,|\,\nabla\varphi\,|^2$ thereby giving

$$\boldsymbol{m}\sim\gamma(\boldsymbol{n})\nabla\varphi+\,|\,\nabla\varphi\,|\,\boldsymbol{P}\nabla_n\gamma(\boldsymbol{n}), \tag{3.15}$$

which is different from equation (3.8) by a factor of γ. As is shown in the electronic supplementary material, the resulting interfacial layer is independent of orientation and is given by the isotropic formula (3.4). This allows the anisotropic surface energy (3.12) to be combined consistently with the phase-field approximation of the Willmore regularization. Our regularized free energy thus reads

$$E[\varphi]=\int_{\Omega}\gamma\frac{1}{\epsilon}\left(f+\frac{\epsilon^2}{2}\,|\,\nabla\varphi\,|^2\right)+\frac{\beta}{2}\frac{1}{\epsilon^3}(f'(\varphi)-\epsilon^2\Delta\varphi)^2\,\mathrm{d}\Omega. \tag{3.16}$$

The phase-field/diffuse-interface evolution equation based on this energy, which, when combined with the asymptotic approximation (3.15), is

$$\frac{\partial \varphi}{\partial t} = \frac{1}{\epsilon} \nabla \cdot (M \nabla \mu), \tag{3.17}$$

$$\mu = \frac{1}{\epsilon}(\gamma f'(\varphi) - \epsilon^2 \nabla \cdot \boldsymbol{m}) + \beta \frac{1}{\epsilon^2}(f''(\varphi)\omega - \epsilon^2 \Delta \omega), \tag{3.18}$$

$$\boldsymbol{m} = \gamma(\boldsymbol{n}) \nabla \varphi + |\nabla \varphi| \boldsymbol{P} \nabla_{\boldsymbol{n}} \gamma(\boldsymbol{n}), \tag{3.19}$$

$$\omega = \frac{1}{\epsilon}(f'(\varphi) - \epsilon^2 \Delta \phi). \tag{3.20}$$

This is now a sixth-order system. We should point out that this evolution does not strictly guarantee that $\mathrm{d}E/\mathrm{d}t \leq 0$ because of the asymptotic approximation (3.15) of $\boldsymbol{m}$. If we did not use this approximation, the energy would be non-increasing. However, the term $f(\varphi)/|\nabla \varphi|$ can be problematic when ϵ is not sufficiently small, since in principle $|\nabla \varphi|$ could vanish in regions where f does not. So using the approximation, we have to check the behaviour of the energy numerically. In all cases, we find that the energy is non-increasing. In the electronic supplementary material, we use the method of matched asymptotic expansions (following Pego 1989; McFadden *et al.* 1993; Leo *et al.* 1998; Loreti & March 2000), which shows that the system (3.17)–(3.20) converges to anisotropic surface diffusion as $\epsilon \to 0$.

4. Numerical methods

To numerically solve the sixth-order system derived in §3, a straightforward modification of the algorithm developed by Wise *et al.* (2007) suffices. We use the mobility and free energy functions given by

$$M(\varphi) = \sqrt{16\varphi^2(1-\varphi)^2 + \tau}, \qquad f(\varphi) = \frac{1}{4}\varphi^2(1-\varphi)^2, \tag{4.1}$$

where τ is a small positive parameter ($\tau = 10^{-6}$) introduced to keep the mobility from vanishing. We solve a coupled system of three second-order equations for φ, μ and ω using second-order accurate-centred finite differences in space. A Crank–Nicholson scheme is used to discretize in time. The anisotropic gradient is discretized in conservation form in space and is lagged in the multigrid V-cycle. To solve the resulting nonlinear equations, a nonlinear multigrid method is used. We further use adaptive block-structured Cartesian mesh refinement (see Wise *et al.* (2007) for details).

5. Numerical results

We begin by comparing the results we have obtained from our new phase-field/diffuse-interface model (3.17)–(3.20) with the sharp-interface model (2.3) at different stages of the evolution in two dimensions. In order to study the sharp-interface model described in §2 dynamically, we use a non-stiff front tracking

technique (e.g. Hou *et al.* 1994; Leo *et al.* 2000; Siegel *et al.* 2004; Li *et al.* 2005). The idea is to use a high-order (spectrally accurate) parametrization of the interface together with a special tangential velocity to enforce dynamic equal spacing in arc length and a non-stiff time integration algorithm for the interface tangent angle.

We consider the evolution of a circle towards equilibrium under surface diffusion with a strong fourfold anisotropy given in equation (2.1), with $\alpha=0.1$, Willmore regularization $\beta=0.01$ and interface thickness parameter $\epsilon=0.03$. The phase-field description of the initial circle is

$$\varphi(x,\, y, t=0) = \frac{1}{2}\left(1.0-\tanh\left(\frac{\sqrt{(x-3.2)^2+(y-3.2)^2}-1.6}{2\sqrt{2}\epsilon}\right)\right). \tag{5.1}$$

The phase-field computational domain is $\Omega=(0,\,6.4)\times(0,\,6.4)$. The simulation is performed with a root-level grid size $h=0.1$ (64×64 grid points); there are two levels of refinement and the finest resolution is $h=0.025$. There are six or seven points across the interface during the simulation. The time step is $s=0.001$. In the sharp-interface model, the parameters α, β and ν are matched to the new phase-field model using the asymptotic formulae in the electronic supplementary material. In the sharp-interface simulation, there are 256 nodes on the interface and the time step size is $s=0.125\times10^{-8}$.

In figure 3, we present snapshots of the evolving $\varphi=0.5$ level set (solid curve) at different times together with the sharp-interface results (dashed curve). The corresponding adaptive meshes and $\varphi=0.5$ level sets are shown in the figure 3(ii). The initial circular interface transforms under the evolution to a fourfold symmetric shape with slightly rounded corners at $t=100$, which is almost the equilibrium shape. There is an excellent agreement between the new phase-field model and the sharp-interface model throughout the evolution. In figure 4, we compare the corresponding energies for the two models, where the scaling of the sharp-interface energy is consistent with the asymptotic formulae in the electronic supplementary material. Both energies are non-increasing in time and there is excellent agreement between the new phase-field (solid curve) and the sharp-interface (dashed curve) results.

Next, we compare the new phase-field model results near equilibrium with the sharp-interface Wulff shape and the regularized Wulff shape near the corner (Spencer 2004). To emphasize the effects of anisotropy, we consider here $\alpha=0.3$. The initial shape is a circle and the domain and all other parameters are the same as in figure 3. We also compare the results of the new phase-field model (figure 5*a*) with previous phase-field models resulting from the classical anisotropy model equation (3.5) combined with either the Willmore regularization (3.11) (figure 5*b*) or the linear regularization (3.10) (figure 5*c*). Observe that the linear regularization not only affects the corner angle but also results in sides that are more curved than the Wulff shape and the Willmore regularization. The $\varphi=0.5$ level curve is plotted at time $t=200$ where the corresponding energy profile in figure 6 suggests that the shapes are nearly equilibrated. The Wulff and regularized shapes are shown as the black and grey dashed curves, respectively. Near the corners, in contrast to the Wulff shape, both the phase-field models with Willmore regularization yield interfaces with smoothed corners, which match the

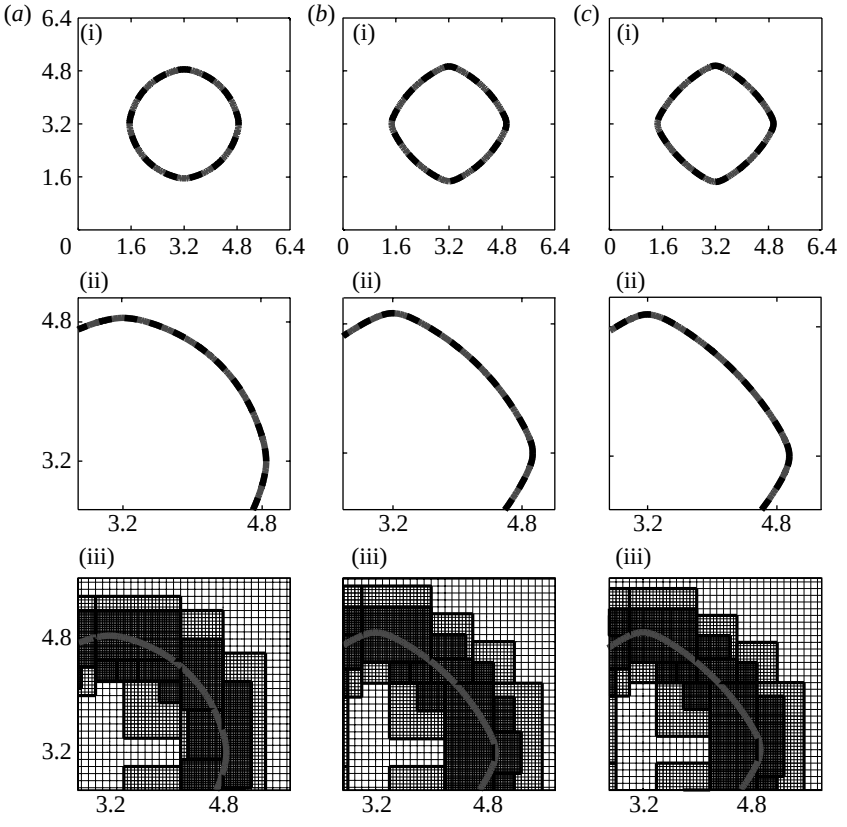

Figure 3. (i) The snapshots of the evolving interface, $\varphi=0.5$ level set, at (*a*) $t=10$, (*b*) $t=50$ and (*c*) $t=100$ (solid curve) in comparison with the sharp-interface result (dashed curve). (ii) Close-up, (iii) mesh snapshot of the diffuse-interface model showing two levels of refinement (finest $h=0.025$). The parameters are given in the text; the initial shape is a circle (equation (5.1)).

regularized Wulff shape. This is the first time we are aware of that such a comparison has been performed in the phase-field/diffuse-interface context. For the new model, away from the corners, there is very good agreement between the numerical results and Wulff shape. But there is a mismatch between the numerical results from previous phase-field models and Wulff shape away from the corners. It seems that the angle between the two sides is larger in these models than that in the Wulff shape. This deviation is real and is not due to the possibility that the shape is still evolving since the energy (shown in figure 6) indicates that the shape is very close to equilibrium. To quantify the deviation, in figure 7, we examine the orientation angle θ (tangent angle) as a function of arc length s near the corner. Observe that the new and previous phase-field models with Willmore regularization match the regularized Wulff shape (Spencer 2004) at the corner, where $\theta=0$, but away from the corner only the new model matches the asymptotic solution and hence the Wulff angle. The previous phase-field model with the linear regularization gives a different result both near and away from the corner. Note that the (Wulff) angle between the two corner sides in the shapes from figure 5 is equal to $\pi-[\max(\theta)-\min(\theta)]$. The deviation between the previous models and the Wulff angle is apparent.

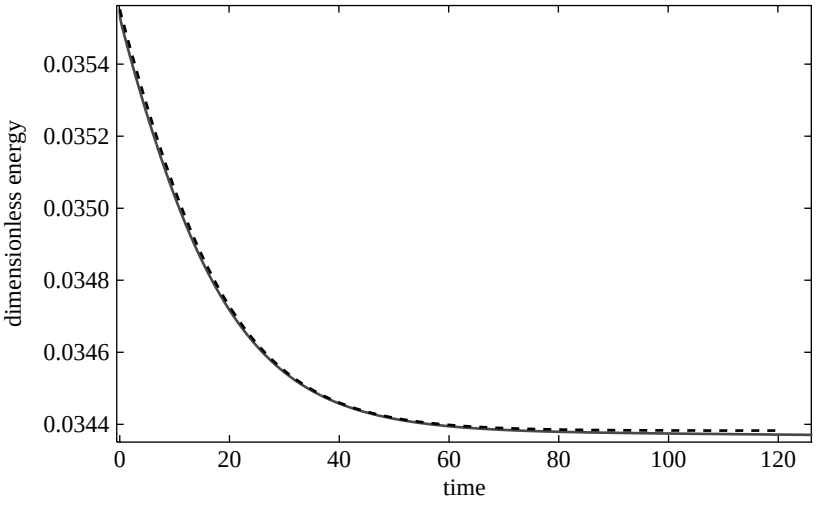

Figure 4. Energy as a function of time for the new phase-field model (solid curve) and the sharp-interface model (dashed curve), for the simulation reported in figure 3. The energy graph suggests that the systems are very close to equilibrium by time $t=100$.

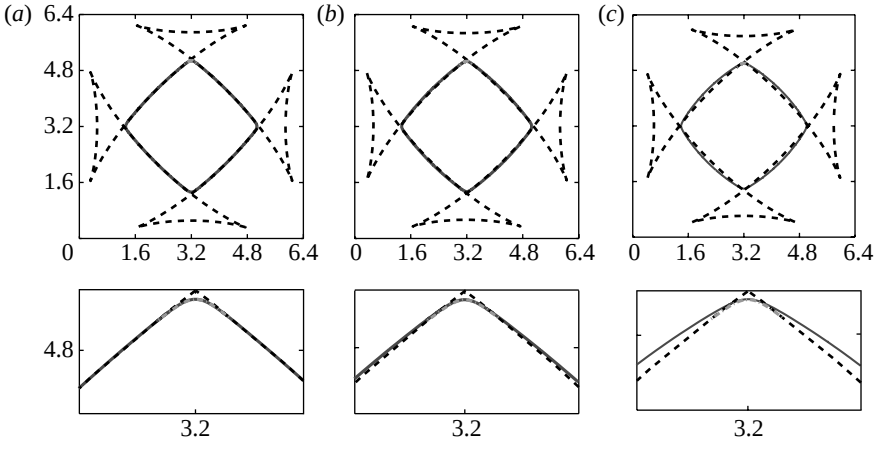

Figure 5. (Top row) The snapshot of the $\varphi=0.5$ level set at $t=200$, the near-equilibrium solution based on the energy profile given in figure 7, (*a*) for the new phase-field interface model (solid curve), and the previous phase-field models with (*b*) Willmore and (*c*) linear regularizations (solid curves). The models are also compared with the Wulff shapes (black dashed curve) and regularized Wulff shape (Spencer 2004) near the corner (grey dashed curve). (Bottom row) Corresponding close-ups. The parameters are given in the text.

In figure 6, the energy is shown for the new (solid curve) and previous phase-field models with Willmore (dashed curve) and linear (dot-dashed curve) regularizations. The total energy for all the models is decreasing. At $t=40$, the decrease in energy becomes very small and after some time the energy is almost constant. Thus, we consider $t=200$ to be very close to equilibrium. Also note that the energies for the previous models are larger than that of the new model, with the linear regularization being quite a bit larger. It is interesting to look at

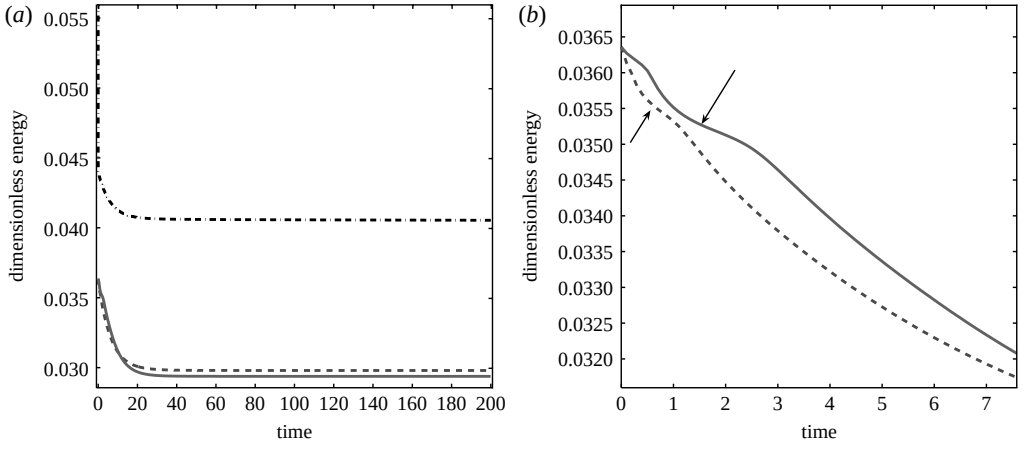

Figure 6. (*a*) Energy profiles for the new (solid curve) and the previous phase-field models with Willmore (dashed curve) and linear (dot-dashed curve) regularizations. The parameters are given in the text. The energy plot suggests that the system is very close to equilibrium by time $t=200$. (*b*) A close-up, with arrows indicating times where energy decrease is slow.

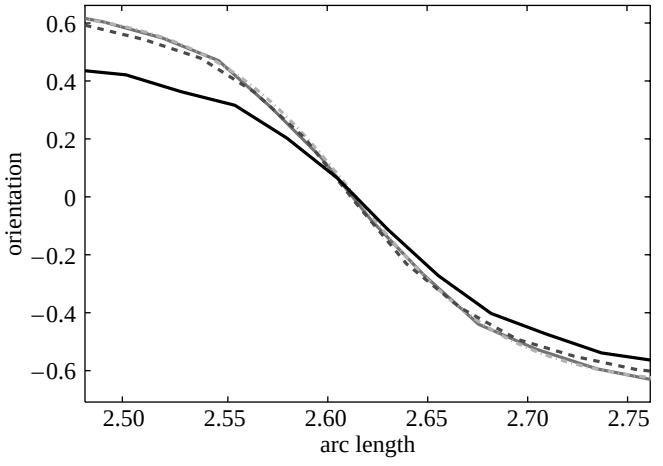

Figure 7. The orientation angle θ is plotted as a function of arc length s at the top corner from the shapes in figure 5 at time $t=200$. The results from the new and previous phase-field models are plotted together with the sharp-interface asymptotic solution for the regularized corner (Spencer 2004). The parameters are given in the text. Grey solid curve, new model; dot-dashed curve, regularized Wulff result; dashed curve, previous model with Willmore regularization; black solid curve, previous model with linear regularization.

the energy at early times (figure 6*b*) where the energies for the models with Willmore regularization are shown. As indicated by arrows, there is a short period of time where the rate of decrease in energy is fairly small. Right before this time, there is a rapid drop in the energy. This phenomenon occurs in all the phase-field models so we focus only on the new model here. As we show, this rapid decrease is associated with the morphological evolution of the shape. In figure 8, snapshots from the evolution of the initially circular shape are shown at early times. By time $t=1.5$, a three-hill/two-valley structure is formed.

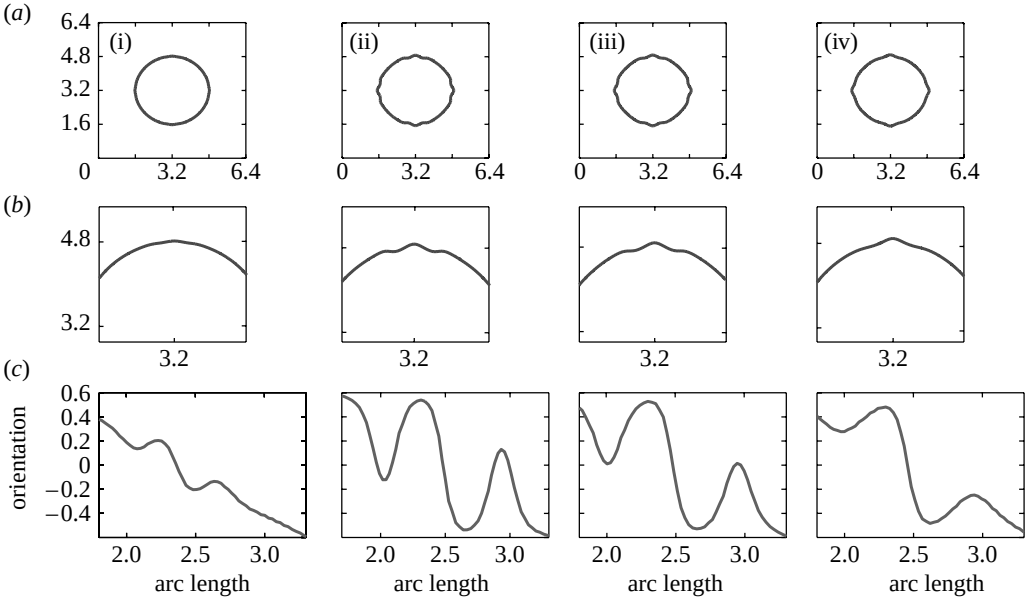

Figure 8. The early time evolution of the initially circular shape towards the equilibrium shape shown in figure 5*a*. (*a*) The shapes, (*b*) a close-up of the top corner region and (*c*) the orientation (tangent angle) as a function of arc length for the top corner region of the shape. (i) Time=0.5, (ii) time=1.5, (iii) time=2.5 and (iv) time=3.5.

This is seen clearly in the close-up and orientation plots shown in figure 8*b*,*c*. Note that the hills and valleys correspond to the points where $\theta=0$; in our orientation $\partial_s\theta<0$ at $\theta=0$ corresponds to a hill. This hill–valley structure emerges because the strong thermodynamic driving force to remove the high-energy orientations on the circular interface creates instability, manifest by the hill–valley structure, which is mediated by the (Willmore) regularization. The drop in the energy seen in figure 6*b* before the arrow corresponds to the formation of the hill–valley structure. Next, the hill–valley structure further evolves to form the single hill structure seen at $t=3.5$; the energy decreases slowly during this process. To characterize this in more detail, we plot in figure 9 the x coordinates of the hills (circles) and valleys (pluses) at different times. A single hill forms first by $t=0.4$. Then, by $t=0.8$, the three-hill/two-valley structure emerges. Then, shortly after $t=1.5$, the hill and valley located around $x\approx2.8$ merge leaving a two-hill/one-valley structure remaining. The hill and valley located near $x\approx3.6$ then merge just after $t=1.9$ leaving the single hill located at $x\approx3.2$.

We now investigate the effect of the Willmore regularization parameter β on the equilibrium interface morphologies using the new phase-field model. We consider three different values, $\beta=0.004$, 0.01 and 0.018. The other parameters are $\alpha=0.1$ and $\epsilon=0.03$. The mesh and time step are the same as in the previous simulations. Using the energy as a guide (not shown), we use the time $t=100$ shapes as approximations of equilibrium. The near-equilibrium $\varphi=0.5$ level curves at $t=100$ are shown in figure 10*a*. The evolution from an initially circular shape to these shapes is similar to that shown in figure 8, but as β decreases sharper and smaller corners form in the equilibrium morphologies. This is further

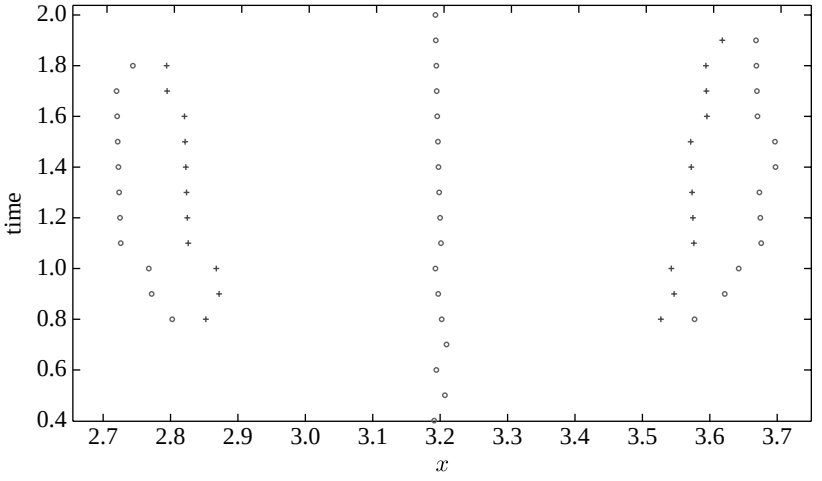

Figure 9. The x coordinates of the hills (circles) and valleys (pluses) shown in figure 8 at different times.

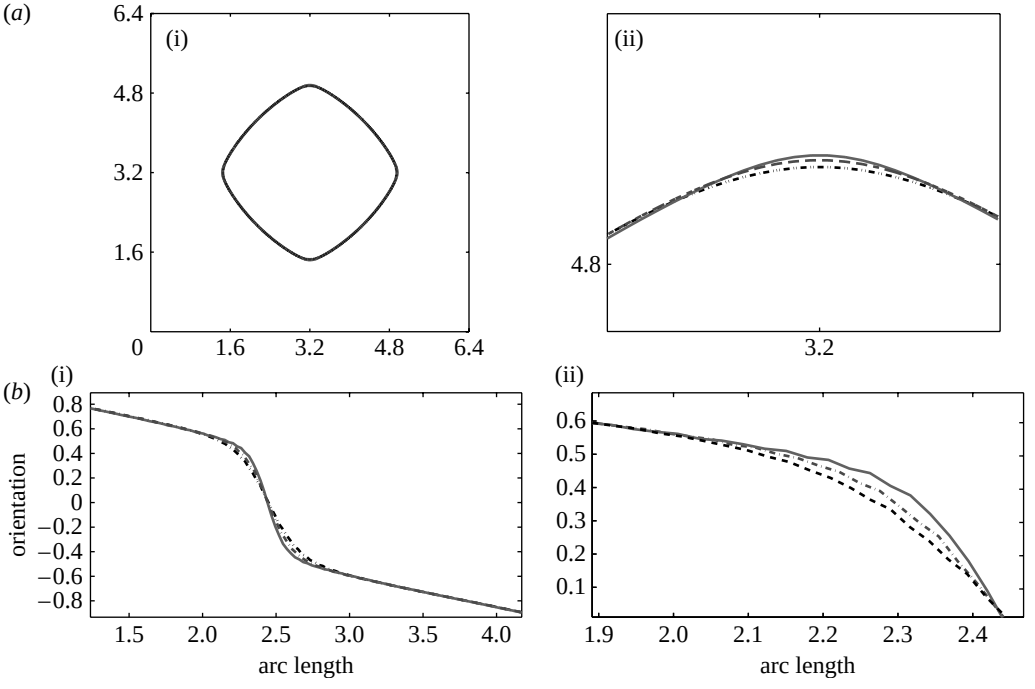

Figure 10. The effect of Willmore regularization β on the corner shape (time=200). (a(i), (ii)) Near-equilibrium $\varphi=0.5$ level curves for the new phase-field model corresponding to the three values of $\beta=0.004$ (solid curve), 0.010 (dot-dashed curve) and 0.018 (dashed curve); (b(i), (ii)) interface orientation (tangent angle) near the top corner for the different β. (ii) Close-ups of each corresponding quantity are shown.

quantified by the plot of the interface orientation angle in figure 10b. Away from the corner, the corresponding three interfaces merge to a shape that matches the sharp-interface Wulff shape.

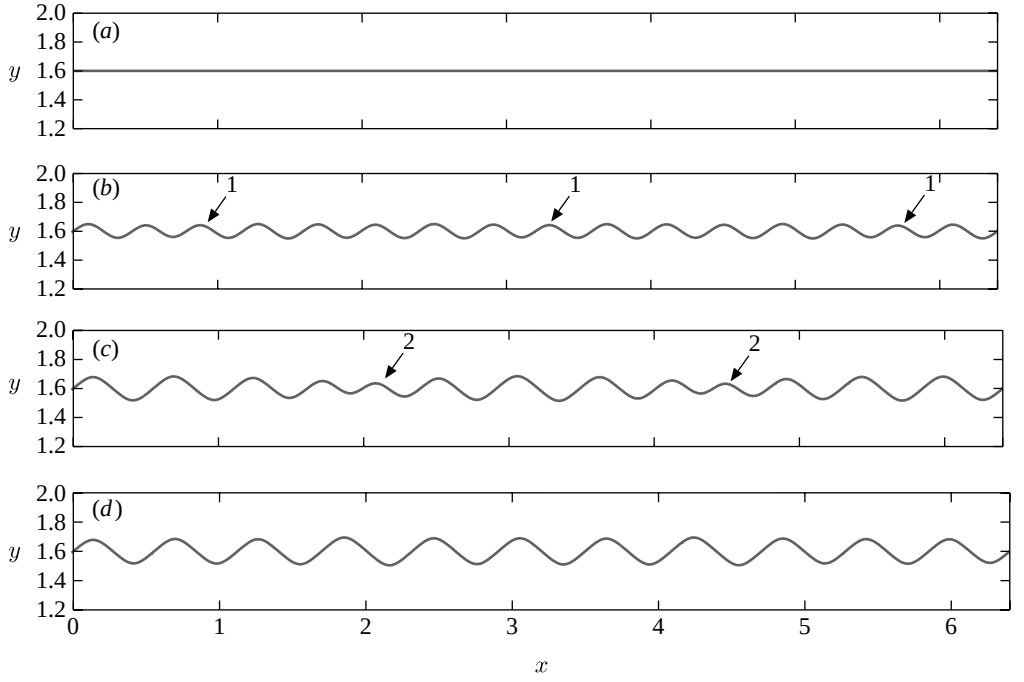

Figure 11. The early time evolution of the $\varphi=0.5$ level curves for open, periodic two-dimensional interfaces ((*a*) time=0.0, (*b*) time=0.5, (*c*) time=2.0, (*d*) time=3.0). The arrows show the sequence in which the hills disappear.

In figure 11, we consider the evolution of a two-dimensional model of a thin film geometry using the new phase-field model. In particular, the evolution of an open, initially flat interface with periodic boundary conditions is shown. The initial geometry is given as

$$\varphi(x,\, y) = \frac{1}{2}\left(1-\tanh\left(\frac{y-1.6}{2\sqrt{2}\epsilon}\right)\right). \tag{5.2}$$

The domain is $\Omega=(0,\, 6.4)\times(0,\, 3.2)$. The fourfold anisotropy parameter is $\alpha=0.5$, the regularization parameter is $\beta=0.01$ and the interface thickness parameter is $\epsilon=0.03$. The mesh parameters are the same as in previous simulations.

In figure 11, the $\varphi=0.5$ level curves are shown at early times during the evolution. Initially, the flat interface decomposes into a hill–valley structure as the interface tries to rid itself of high-energy orientations. This corresponds to a rapid decrease in energy as seen in figure 12 and this process is similar to that described earlier for closed shapes. As the system evolves, the hill–valley structure begins to coarsen as hills and valleys are removed from the system. The arrows in figure 11 indicate the sequence in which the hills and valleys are removed. As seen from figure 12*b*, these coarsening events are associated with rapid drops in the energy. To investigate the coarsening process in more detail, we consider the interface orientation angle θ. In figure 13, we observe that the hill–valley structures with the smallest $[\max(\theta)-\min(\theta)]$ disappear first, i.e. those with wider corner angles. In particular, the hills marked by 1 at $t=0.5$

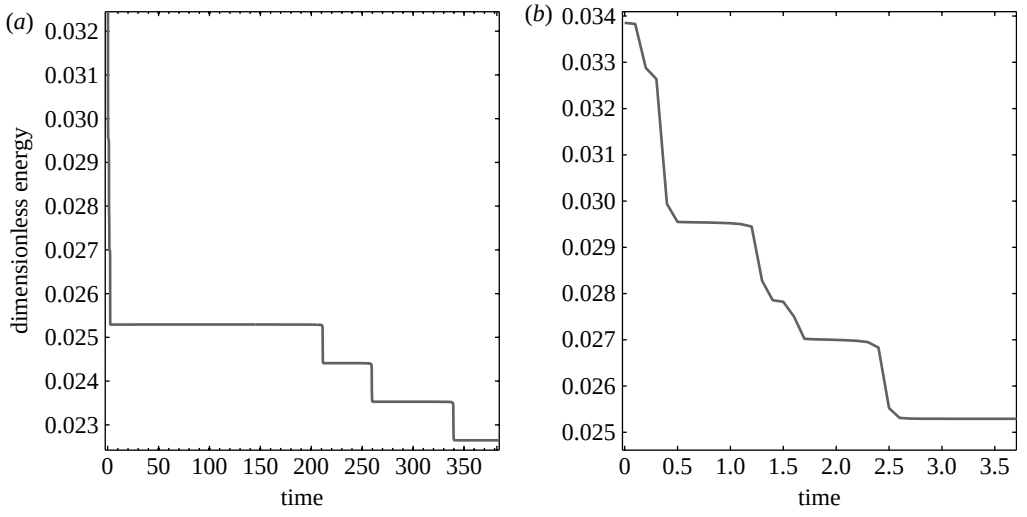

Figure 12. (*a*) The energy evolution corresponding to the simulation using an open, periodic two-dimensional interface from figure 11. The rapid drops correspond to the loss of a hill–valley structure during coarsening. (*b*) A close-up of the early time evolution.

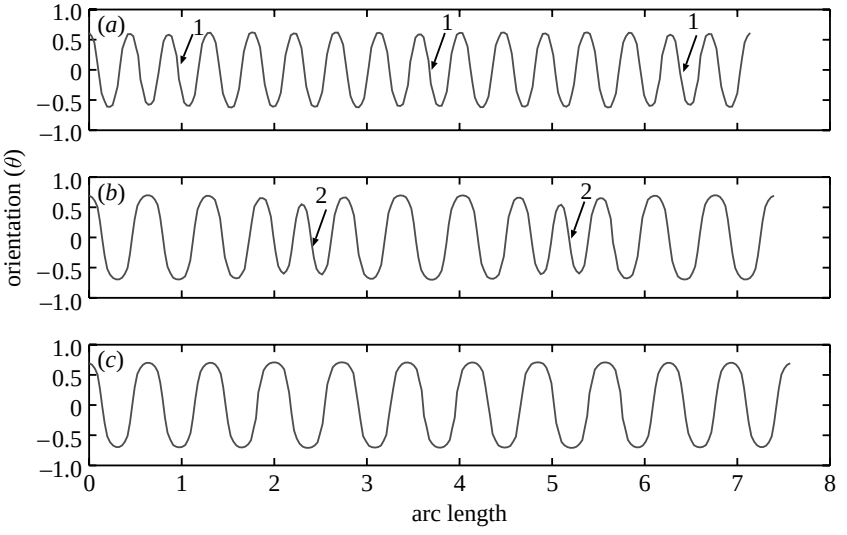

Figure 13. The orientation angle (tangent angle) as a function of arc length at different times for the simulation shown at early times in figure 11 ((*a*) $t=0.5$, (*b*) $t=2.0$, (*c*) $t=3.0$). The arrows indicate the sequence in which the peaks disappear.

disappear earlier than the other hills. Next, the hills marked with 2 at time $t=2.0$ disappear. At longer times, the coarsening process is shown in figure 14 where the x coordinates of the hills (circles) and valleys (pluses) are shown at different times. As seen in the figure, the coarsening process may occur symmetrically by either two hills merging with a valley to produce a hill or by two valleys merging with a hill to produce a valley. As the interface coarsens, both the hills and the

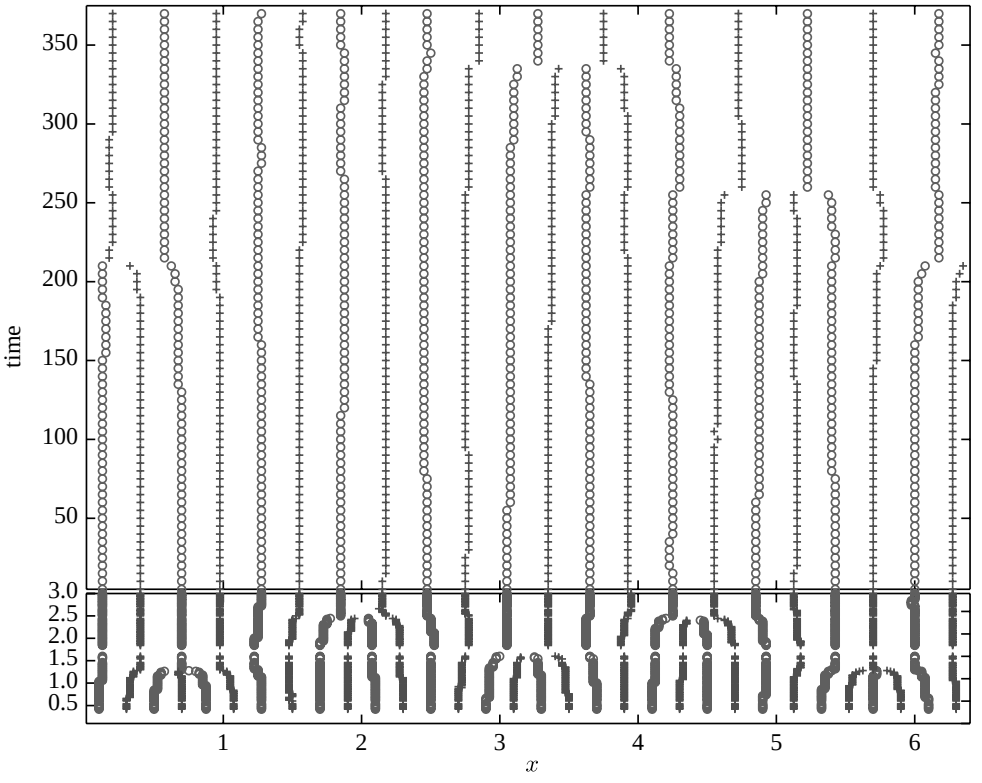

Figure 14. The x coordinates of hills (circles) and valleys (pluses) at different times for the simulation shown at early times in figure 11.

valleys tend to match the regularized Wulff shape (Spencer 2004). This symmetry (e.g. the shape of a hill is the inversion of that of a valley) is seen in figure 15*a* where the orientation angle for the new phase-field model is shown at a late time $t=350$ (solid curve) together with the asymptotic form of the sharp-interface Willmore regularization (dashed curve) from Spencer (2004). Note that three of the hill–valley structures have smaller $[\max(\theta)-\min(\theta)]$ values than the others. These are the next to coarsen, although the process takes a very long time. The corresponding interface morphology is shown in figure 15*b*. We further note that symmetry in both the coarsening process and the shapes of the hills and valleys may be broken when additional effects are considered, such as deposition or elastic forces (e.g. Hausser & Voigt 2005*b*; Zhou *et al.* 2008).

We next turn to three dimensions. In figure 16, the evolution of an initially spherical shape towards the Wulff shape is shown, using the new phase-field model with $\alpha=0.3$, $\beta=0.01$ and $\epsilon=0.03$. Observe that the Wulff shape resembles a double-sided pyramid. The computational domain is $\Omega=(0, 3.2)\times(0, 3.2)\times(0, 3.2)$. The simulation is performed with a root-level grid of $32\times32\times32$ (with mesh size $h=0.1$) and there are two levels of refinement. The resolution on the finest mesh is $h=0.025$ and the time step size $s=0.001$. As in two dimensions, there are approximately six or seven mesh points across the interface during the

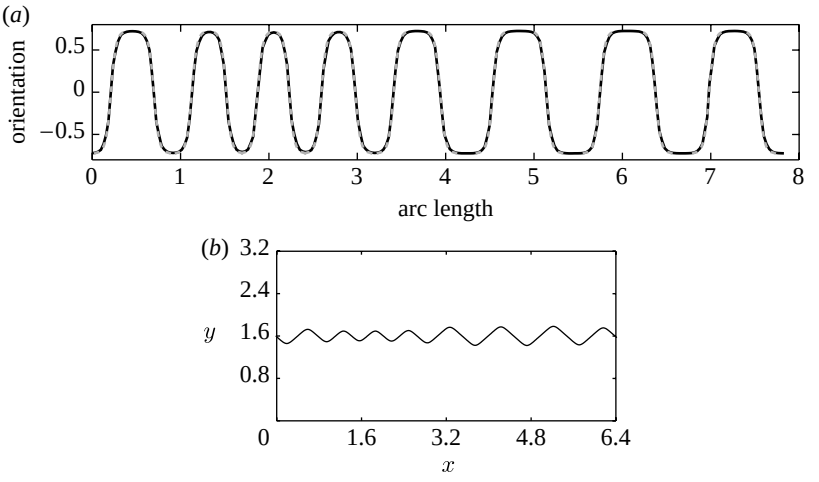

Figure 15. A late-time ($t=350$) open, periodic interface continued from that shown in figure 11. (*a*) The orientation angle as a function of arc length for the new phase-field model (solid curve) and the asymptotic solution for the Willmore regularization (Spencer 2004; dashed). (*b*) The corresponding $\varphi=0.5$ level curve.

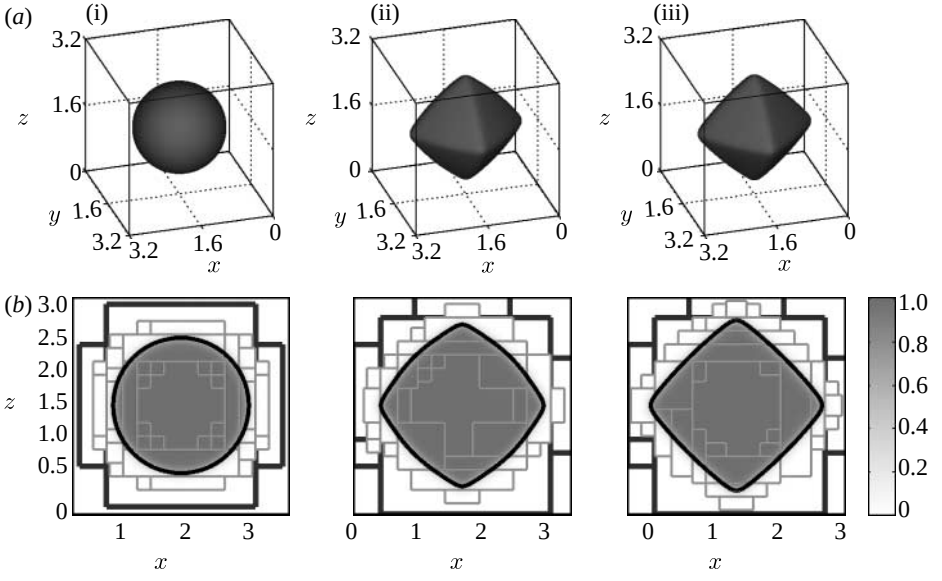

Figure 16. The three-dimensional evolution of an initially spherical surface at three times: (i) $t=0$, (ii) $t=2$ and (iii) $t=20$. (*a*) The $\varphi=0.5$ surface, (*b*) the $y=1.6$ slice together with the slices of the bounding boxes of the three-dimensional adaptive mesh. There are two levels of refinement and each interior box contains a mesh that is one-half of the size of the box that contains it.

simulation. In figure 16*a*, the $\varphi=0.5$ surface is plotted. In figure 16*b*, the $y=1.6$ slice is shown together with the corresponding slices of the bounding boxes of the three-dimensional adaptive mesh. Each box contains a mesh that is one-half of the size of that in the box that contains it.

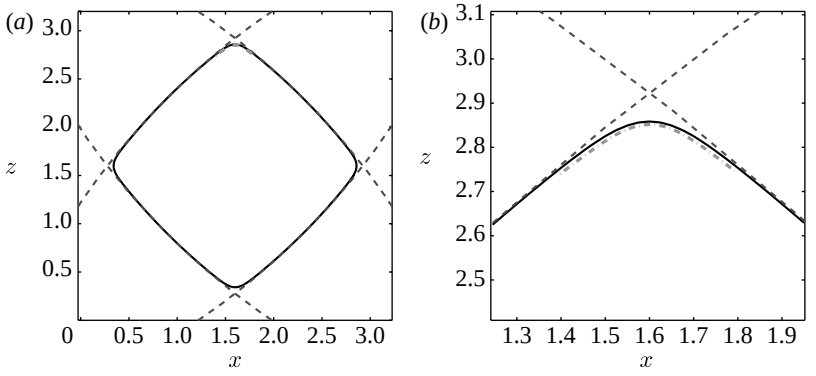

Figure 17. (*a*) The slice of three-dimensional shape as shown in figure 16 in comparison with Wulff and regularized Wulff shapes and (*b*) close-up (solid curve, contour=0.5; dashed curve, Wulff shape; dot-dashed curve, regularized Wulff result).

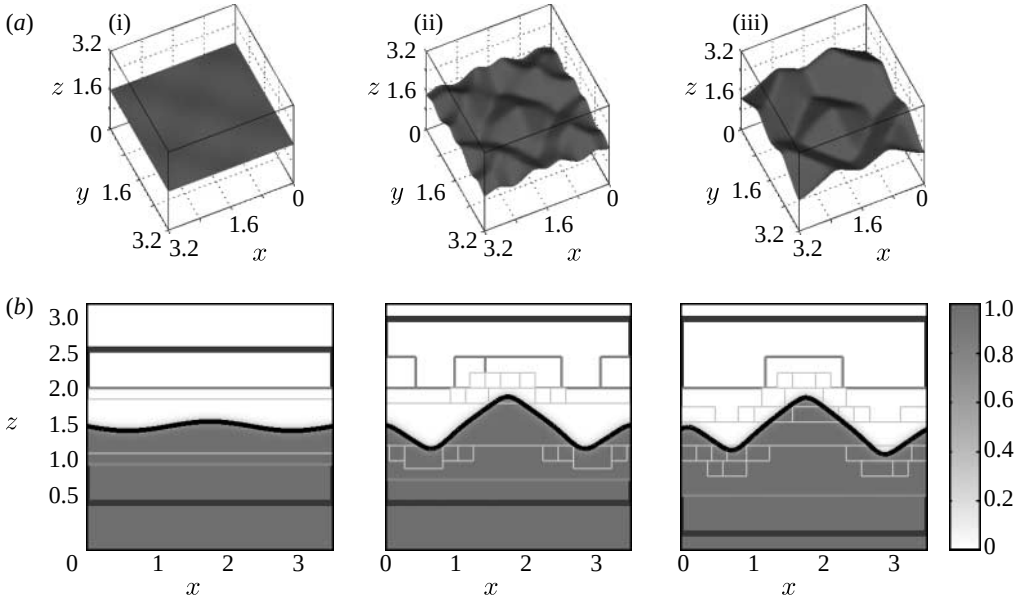

Figure 18. The three-dimensional evolution of a slightly perturbed, open periodic three-dimensional surface. (*a*) The $\varphi=0.5$ surface at times (i) $t=0$, (ii) $t=4$ and (iii) $t=40$ and (*b*) the corresponding $y=1.6$ slices together with the slices of the bounding boxes from the three-dimensional adaptive mesh.

In figure 17, we compare the $y=1.6$ slice (solid curve) at $t=20$ with the corresponding slice of the three-dimensional Wulff shape (dashed curve; which also corresponds to the two-dimensional Wulff shape since the slice is through the centre of the three-dimensional shape), and also with the asymptotic Willmore regularized solution (dot-dashed curve; Spencer 2004). As in two dimensions, away from the corner, there is excellent agreement between the Wulff shape and the result from the new phase-field model. Near the corner, there is excellent agreement with the asymptotic solution.

In figure 18, we present a final three-dimensional example corresponding to an open, periodic three-dimensional interface, which serves as a model for a thin film. The new phase-field model is used with $\alpha=0.3$, $\beta=0.01$ and $\epsilon=0.024$. The computational domain is $\Omega=(0, 3.2)\times(0, 3.2)\times(0, 3.2)$. The simulation is performed with a root-level grid of $16\times16\times16$ (with mesh size $h=0.2$). There are three levels of refinement. The finest resolution is $h=0.025$ and the time step size $s=0.001$. There are approximately six mesh points across the interface during the simulation. In figure 18*a*, the $\varphi=0.5$ surface is plotted at time $t=40$; in figure 18*b*, the corresponding $y=1.6$ slices are shown together with the slices of the bounding boxes of the three-dimensional adaptive mesh. As in two dimensions, the slightly perturbed initial interface rapidly decomposes into a hill–valley structure that coarsens leaving a central smoothed pyramid surrounded by a periodic hill–valley structure. A comparison (not shown) indicates that the $y=1.6$ slices of the hills and valleys match the sharp-interface theory of Spencer (2004).

6. Conclusion

We have presented a new phase-field model for strongly anisotropic crystal growth using regularized, anisotropic Cahn–Hilliard-type equations. A new formulation was used for the anisotropic surface energy and the regularization was performed using a phase-field/diffuse-interface approximation of the Willmore energy (square of the mean curvature). A key feature of our approach was that the interface thickness is independent of orientation. This removed an incompatibility between the anisotropy and the Willmore regularization proposed and used in earlier phase-field models. An asymptotic analysis presented in the electronic supplementary material demonstrates the convergence of the new phase-field model to the sharp-interface model. We presented two- and three-dimensional numerical results using an adaptive, nonlinear multigrid finite-difference method. We found excellent agreement between the new phase-field and the sharp-interface dynamics. The computed equilibrium shapes using the Cahn–Hilliard approach also match a recently developed analytical sharp-interface theory that describes the rounding of the sharp corners by the Willmore regularization.

In the future, we will extend the model described here to simulate heteroepitaxial thin film growth. We will incorporate deposition, misfit strain, a substrate and wetting effects. Through continued improvements in the efficiency of the numerical algorithm, we plan to study the long-time coarsening of thin film systems. In addition, one of the important problems we seek to address is the control of the formation and coarsening of nanoscale structures to achieve desired spatial orderings.

It is a pleasure to thank Katsuyo Thornton and Peter Voorhees for their valuable discussions. We especially thank Shuwang Li for assistance with the sharp-interface simulations. It is a pleasure to thank Andreas Rätz. We gratefully acknowledge the financial support of the National Science Foundation, Divisions of Materials Research (DMR) and Mathematical Sciences (DMS), the European Union through EU grant no. STRP 016447 'MagDot' and the German Science Foundation.

References

Biben, T. & Misbah, C. 2003 Tumbling of vesicles under shear flow with an advected field approach. *Phys. Rev. E* **67**, 031908. (doi:10.1103/PhysRevE.67.031908)

Biben, T., Kassner, K. & Misbah, C. 2005 Phase-field approach to three-dimensional vesicle dynamics. *Phys. Rev. E* **72**, 049121. (doi:10.1103/PhysRevE.72.041921)

Burger, M., Hausser, F., Stöcker, C. & Voigt, A. 2007 A level set approach to anisotropic flows with curvature regularization. *J. Comput. Phys.* **225**, 183–205. (doi:10.1016/j.jcp.2006.11.026)

Cahn, J. W. & Hilliard, J. 1958 Free energy of a non-uniform system: interfacial free energy. *J. Chem. Phys.* **28**, 258–267. (doi:10.1063/1.1744102)

Cahn, J. W. & Hoffman, D. W. 1974 A vector thermodynamics for anisotropic surfaces-II. Curved and faceted surfaces. *Acta Metall.* **22**, 1205–1214. (doi:10.1016/0001-6160(74)90134-5)

Cahn, J. W., Elliott, C. M. & Novick-Cohen, A. 1996 The Cahn–Hilliard equation with a concentration dependent mobility: motion by minus the Laplacian of the mean curvature. *Eur. J. Appl. Math.* **7**, 287–302. (doi:10.1017/S0956792500002369)

De Giorgi, E. 1991 Some remarks on gamma-convergence and least squares methods. In *Composite media and homogeneization theory*, vol. 5 (eds G. Dal Maso & G. F. Dell'Antonio). *Progress in nonlinear differential equations and their applications*, pp. 135–142. Boston, MA: Birkhauser.

DiCarlo, A., Gurtin, M. & Podio-Guidugli, P. 1992 A regularized equation for anisotropic motion-by-curvature. *SIAM J. Appl. Math.* **52**, 1111–1119. (doi:10.1137/0152065)

Du, Q., Liu, C. & Wang, X. 2004 A phase field approach in the numerical study of the elastic bending energy for vesicle membranes. *J. Comput. Phys.* **198**, 450–468. (doi:10.1016/j.jcp.2004.01.029)

Du, Q., Liu, C., Ryhman, R. & Wang, X. 2005 A phase field formulation of the Willmore problem. *Nonlinearity* **18**, 1249–1267. (doi:10.1088/0951-7715/18/3/016)

Eggleston, J. J. & Voorhees, P. W. 2002 Ordered growth of nanocrystals via a morphological instability. *Appl. Phys. Lett.* **80**, 306–308. (doi:10.1063/1.1429757)

Eggleston, J. J., McFadden, G. & Voorhees, P. W. 2001 A phase-field model for highly anisotropic interfacial energy. *Physica D* **150**, 91–103. (doi:10.1016/S0167-2789(00)00222-0)

Fried, E. & Gurtin, M. E. 2004 A unified treatment of evolving interfaces accounting for small deformations and atomic transport with emphasis on grain-boundaries and epitaxy. *Adv. Appl. Mech.* **40**, 1–177. (doi:10.1016/S0065-2156(04)40001-5)

Gugenberger, C., Spatschek, R. & Kassner, K. 2008 Comparison of phase-field models for surface diffusion. *Phys. Rev. E* **78**, 016703. (doi:10.1103/PhysRevE.78.016703)

Gurtin, M. E. & Jabbour, M. 2002 Interface evolution in three dimensions with curvature-dependent energy and surface diffusion: interface-controlled evolution, phase transitions, epitaxial growth of elastic films. *Arch. Ration. Mech. Anal.* **163**, 171–208. (doi:10.1007/s002050200193)

Hausser, F. & Voigt, A. 2005*a* A discrete scheme for regularized anisotropic surface diffusion: a 6th order geometric evolution equation. *Interfaces Free Bound.* **7**, 353–369.

Hausser, F. & Voigt, A. 2005*b* Facet formation and coarsening modeled by a geometric evolution law for epitaxial growth. *J. Cryst. Growth* **275**, e47–e51. (doi:10.1016/j.jcrysgro.2004.10.137)

Herring, C. 1951 Some theorems on the free energies of crystal surfaces. *Phys. Rev.* **82**, 87–93. (doi:10.1103/PhysRev.82.87)

Hou, T. Y., Lowengrub, J. S. & Shelley, M. J. 1994 Removing the stiffness from interfacial flows with surface tension. *J. Comput. Phys.* **114**, 312–338. (doi:10.1006/jcph.1994.1170)

Jamet, D. & Misbah, C. 2008 Toward a thermodynamically consistent picture of the phase-field model of vesicles: curvature energy. *Phys. Rev. E* **78**, 031902. (doi:10.1103/PhysRevE.78.031902)

Kobayashi, R. 1993 Modeling and numerical simulations of dendritic crystal growth. *Physica D* **63**, 410–423. (doi:10.1016/0167-2789(93)90120-P)

Leo, P. H., Lowengrub, J. S. & Jou, H. J. 1998 A diffuse interface model for microstructural evolution in elastically stressed solids. *Acta Metall.* **46**, 2113–2130. (doi:10.1016/S1359-6454(97)00377-7)

Leo, P. H., Lowengrub, J. S. & Nie, Q. 2000 Microstructural evolution in orthotropic elastic media. *J. Comput. Phys.* **157**, 44–88. (doi:10.1006/jcph.1999.6359)

Li, S., Lowengrub, J. S. & Leo, P. H. 2005 Nonlinear morphological control of growing crystals. *Physica D* **208**, 209–219. (doi:10.1016/j.physd.2005.06.021)

Liu, F. & Metiu, H. 1993 Dynamics of phase separation of crystal surfaces. *Phys. Rev. B* **48**, 5808–5817. (doi:10.1103/PhysRevB.48.5808)

Loreti, P. & March, R. 2000 Propagation of fronts in a nonlinear fourth order equation. *Eur. J. Appl. Math.* **11**, 203–213. (doi:10.1017/S0956792599004131)

McFadden, G. B., Wheeler, A. A., Braun, R. J., Coriell, S. R. & Sekerka, R. F. 1993 Phase-field models for anisotropic interfaces. *J. Phys. Rev. E* **48**, 2016–2024. (doi:10.1103/PhysRevE.48.2016)

Pego, R. 1989 Front migration in the nonlinear Cahn–Hilliard equation. *Proc. R. Soc. A* **422**, 261–278. (doi:10.1098/rspa.1989.0027)

Rätz, A. & Voigt, A. 2006 Higher order regularization of anisotropic geometric evolution equations in three dimensions. *J. Comput. Theor. Nanosci.* **3**, 560–564.

Rätz, A., Ribalta, A. & Voigt, A. 2006 Surface evolution of elastically stressed films under deposition by a diffuse interface model. *J. Comput. Phys.* **214**, 187–208. (doi:10.1016/j.jcp.2005.09.013)

Röger, M. & Schätzle, R. 2006 On a modified conjecture of DeGiorgi. *Mathematische Zeitschrift* **254**, 675–714. (doi:10.1007/s00209-006-0002-6)

Savina, T. V., Golovin, A. A., Davis, S. H., Nepomnyashchy, A. A. & Voorhees, P. W. 2003 Faceting of a growing crystal surface by surface diffusion. *Phys. Rev. E* **67**, 021606. (doi:10.1103/PhysRevE.67.021606)

Sekerka, R. F. 2005 Analytical criteria for missing orientations on three-dimensional equilibrium shapes. *J. Cryst. Growth* **275**, 77–82. (doi:10.1016/j.jcrysgro.2004.10.069)

Siegel, M., Miksis, M. J. & Voorhees, P. W. 2004 Evolution of material voids for highly anisotropic surface energy. *J. Mech. Phys. Solids* **52**, 1319–1353. (doi:10.1016/j.jmps.2003.11.003)

Spencer, B. 2004 Asymptotic solutions for the equilibrium crystal shape with small corner energy regularization. *Phys. Rev. E* **69**, 011603. (doi:10.1103/PhysRevE.69.011603)

Stewart, J. & Goldenfeld, N. 1992 Spinodal decomposition of a crystal surface. *Phys. Rev. A* **46**, 6505–6512. (doi:10.1103/PhysRevA.46.6505)

Wang, X. 2007 Asymptotic analysis of phase field formulations of bending elasticity models. *SIAM J. Math. Anal.* **39**, 1367–1401. (doi:10.1137/060663519)

Wheeler, A. A. 2006 Phase-field theory of edges in an anisotropic crystal. *Proc. R. Soc. A* **462**, 3363–3384. (doi:10.1098/rspa.2006.1721)

Wheeler, A. A., McFadden, G. B. & Boettinger, W. J. 1996 Phase-field model for solidification of a eutectic alloy. *Proc. R. Soc. A* **452**, 495–525. (doi:10.1098/rspa.1996.0026)

Wise, S. M., Lowengrub, J. S., Kim, J., Thornton, K., Voorhees, P. W. & Johnson, W. 2005 Quantum dot formation on a strain-patterned epitaxial thin film. *Appl. Phys. Lett.* **87**, 133102. (doi:10.1063/1.2061852)

Wise, S. M., Kim, J. & Lowengrub, J. S. 2007 Solving the regularized, strongly anisotropic Cahn–Hilliard equation by an adaptive non-linear multigrid method. *J. Comp. Phys.* **226**, 414–446. (doi:10.1016/j.jcp.2007.04.020)

Zhou, P., Torabi, S., Lowengrub, J. S., Voigt, A. & Wise, S. M. In preparation. Modeling the evolution of strongly anisotropic, misfitting thin films.